[8] Patrick, R. M. and Schneiderman, A. M., "Performance Characteristics of a Magnetic Annular Arc," *AIAA Journal*, Vol. 4, No. 2, Feb. 1966, pp. 283–290.
[9] Rosciszewski, J., "Acceleration Process in the Hall Current Device," *The Physics of Fluids*, Vol. 10, No. 5, May 1967, p. 1095.
[10] Hassan, H. A., Hess, R. V., and Grossman, W., "Study of Coaxial Hall Current Accelerators at Moderate Pressures," TN D-3286, Oct. 1966, NASA.
[11] Workman, J. B., "Arc Structure in a Magnetic Annular Discharge," *AIAA Journal*, Vol. 7, No. 3, March 1969, pp. 512–519.
[12] Allario, F., Jarrett, O., and Hess, R. V., "Onset of Rotating Disturbance in the Interelectrode Region and Exhaust Jet of an MPD Arc," *AIAA Journal*, Vol. 8, No. 5, May 1970, pp. 902–907.
[13] Larson, A. V., "Measurements of Plasma Flow in an MPD Engine," AIAA Paper 69-233, Williamsburg, Va., 1969.
[14] Sidney, B. D., Allario, F., and Hess, R. V., "Onset of Rotating Disturbance in a Linear Hall Current Accelerator," *AIAA Journal*, Vol. 8, No. 6, June 1970, pp. 1117–1120.
[15] Smith, J. M., "Electrothermal Instability—An Explanation of the MPD Arc Thruster Rotating Spoke Phenomenon," AIAA Paper 69-231, Williamsburg, Va., 1969.
[16] Hassan, H. A. and Thompson, C. C., "Onset of Instabilities in Coaxial Hall Current Accelerators," AIAA Paper 69-230, Williamsburg, Va., 1969.
[17] Fay, J. A. and Cochran, R. A., "An Actuator-Disk Model for Azimuthally Non-Uniform MPD Arcs," *AIAA Journal*, Vol. 7, No. 9, Sept. 1969, pp. 1688–1692.
[18] Pugh, E. and Patrick, R., "Plasma Wind Tunnel Studies of Collision-Free Flows and Shocks," *The Physics of Fluids*, Vol. 10, No. 12, Dec. 1967, pp. 2579–2585.
[19] Schneiderman, A. M. and Patrick, R. M., "Axial Current Distribution in the Exhaust of the Magnetic Annular Arc," *AIAA Journal*, Vol. 5, No. 2, Feb. 1967, pp. 249–253.
[20] Roman, W. C. and Myers, T. W., "Experimental Investigation of an Electric Arc in Transverse Aerodynamic and Magnetic Fields," *AIAA Journal*, Vol. 5, No. 11, Nov. 1967, pp. 2011–2017.
[21] Bond, C. E., "Slanting of a Magnetically Stabilized Electric Arc in Transverse Supersonic Flow," *The Physics of Fluids*, Vol. 9, No. 4, April 1966, pp. 705–710.
[22] Winograd, Y. Y. and Klein, J. F., "Electric Arc Stabilization in Crossed Convective and Magnetic Fields," *AIAA Journal*, Vol. 7, No. 9, Sept. 1969, pp. 1699–1703.
[23] Kuethe, A. M., Harvey, R. L., and Nicolai, L. M., "Model of an Electric Arc Balanced Magnetically in a Gas Flow," AIAA Paper 67-96, New York, 1967.
[24] Cowley, M. D., "A Boundary-Layer Model for Balanced Arcs," Fluid Mechanics Lab. Publication 67-6, July 1967, Dept. of Mechanical Engineering, M.I.T., Cambridge, Mass.
[25] Pugh, E. R., Patrick, R. M., and Schneiderman, A. M., "Use of Magnetic Annular Arc Accelerator For High Enthalpy, High Stagnation Pressure Flows," *Proceedings of 8th Symposium on Engineering Aspects of MHD*, Stanford, Calif., 1967.
[26] Cochran, R. A. and Fay, J. A., "Occurrence and Behavior of Current Spokes in MPD Arcs," Fluid Mechanics Lab. Publication 70-1, Feb. 1970, Dept. of Mechanical Engineering, M.I.T., Cambridge, Mass.
[27] Simon, A., "Instability of a Partially Ionized Plasma in Crossed Electric and Magnetic Fields," *The Physics of Fluids*, Vol. 6, No. 3, March 1963, pp. 382–388.
[28] Hoh, F. C., "Instability of Penning-Type Discharge," *The Physics of Fluids*, Vol. 6, No. 8, Aug. 1963, pp. 1184–1191.

MAY 1971 AIAA JOURNAL VOL. 9, NO. 5

Properties of the Rotating Spoke in an Unstable Pulsed MPD Arc

R. KRIBEL,* C. ECKDAHL,† AND R. LOVBERG‡
University of California—San Diego, La Jolla, Calif.

A modified magnetoplasmadynamic (MPD) arc has been operated in a pulsed mode to permit internal probing of the arc region. The arc attains steady-state operation which strongly resembles the behavior of the more conventional continuous MPD arcs. Spatial surveys with magnetic probes and small Rogowski coil probes show the current distribution to have the form of a well defined radial spoke which rotates azimuthally. The rotation frequency is typically about 40 kc with Argon gas. Observations with double plane Langmuir probes measuring plasma flow indicate that the rotating current spoke corresponds to an actual plasma rotation. The spoke exhibits an internal structure. The plasma in the leading edge is streaming radially outward, while that in the trailing edge is counterstreaming inward towards the cathode. Most of the arc current flows in the trailing section, and the ions there seem to carry about 30% of the total arc current.

I. Introduction

THE magnetoplasmadynamic (MPD) arc has been found to be a very efficient device for converting electrical power into directed propellant kinetic energy.[1–5] Most of the early MPD research was concerned with optimization of the arc for propulsion use, which implies an emphasis on thrust, specific impulse and efficiency. Since these parameters can be determined by measurements external to the arc itself there was little motivation to investigate the precise internal character of the arc. In recent years it has become apparent that the MPD arc is indeed a complicated device requiring much more detailed information if a fundamental understanding of its operation and ultimate capabilities is to be achieved. The intent of the work discussed in this paper is to make a detailed study of the internal arc region and hopefully determine some of the more important processes which might affect the over-all arc performance. No attempt has been made to measure thrust or efficiency directly. Internal arc studies are difficult in conventional MPD arcs because of the very high power density in the current channel

Presented as Paper 69-234 at the AIAA 7th Electric Propulsion Conference, Williamsburg, Va., March 3–5, 1969; submitted April 7, 1969; revision received September 17, 1970. This work was supported by NASA Grant NGR-009-030. The authors wish to express their thanks to the entire Plasma Physics Group at UCSD and especially to H. Davis and D. Nyman for their help and stimulating discussions. The technical assistance of J. Moyta proved invaluable during the experiment.

* Research Assistant, Department of Physics; now Assistant Professor, Department of Physics, Drake University, Des Moines, Iowa.
† Research Assistant, Department of Physics.
‡ Professor of Physics.

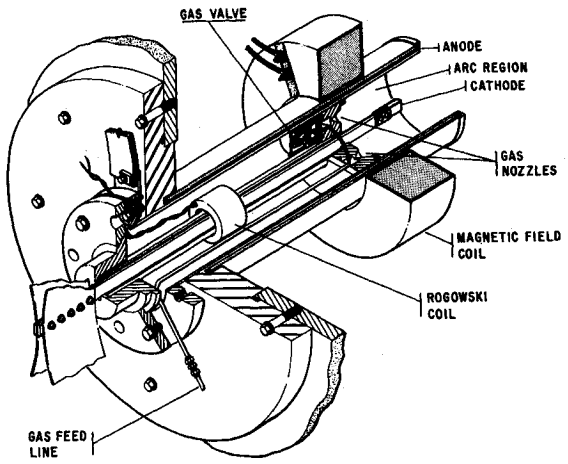

Fig. 1 Cutaway view of MPD arc used in this experiment.

and because of the small physical dimensions of the discharge region. These problems have been avoided by 1) operating the arc in short pulses so that the cumulative heat loading on probes is not destructive and 2) designing the system with a relatively large open coaxial electrode structure so that the spatial resolution of reasonably-sized probes is a small fraction of the interelectrode spacing. Both modifications have been adopted with considerable caution.

The pulsed arc can achieve true steady-state operation characteristic of the conventional MPD arcs, only if all of the time constants of the system are short compared to the length of the operating pulse. For a pulse length of 500 μsec, this condition seems to be violated only by the thermal heating time constant of the tungsten cathode. In the steady-state arcs the cathode temperature approaches the melting point of tungsten in a time interval of the order of seconds. The thermionic electrons produced by the hot cathode surface are apparently necessary for the attainment of typical MPD arc behavior. This difficulty has been overcome in the pulsed arc by preheating the cathode surface to approximately 3400°K. For this purpose a U-shaped tungsten ribbon is attached to the end of the cathode and heated by passing several thousand amperes of current through it just prior to the main arc pulse.

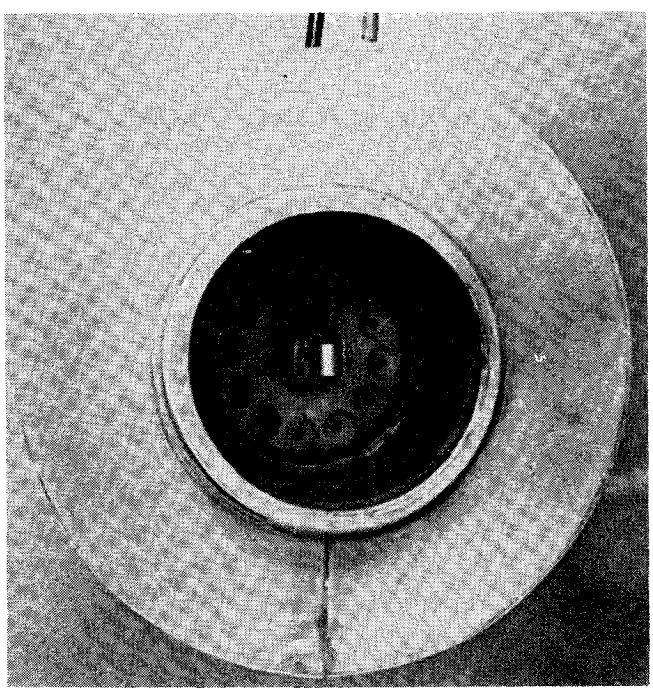

Fig. 2 Muzzle view of MPD accelerator.

II. Experimental Apparatus

A. Accelerator Design

The pulsed MPD arc used in this experiment is shown in the cutaway drawing of Fig. 1. The electrodes consist of two coaxial stainless steel cylinders. The outer electrode, which is the anode, has an inside diameter of 8.7 cm. The cathode is a 2-cm-diam rod with a U-shaped tungsten filament mounted on the end. The cathode rod is split longitudinally into two sections to permit preheating of the filament. The diverging magnetic field is produced by the bias field coil, which is mounted on the outside surface of the anode. The Rogowski coil on the cathode rod is used to measure the total arc current.

Figure 2 is a muzzle view of the accelerator in which the electrodes, bias field coil, and input gas nozzles are clearly visible.

The input gas flow is also pulsed but is permitted to reach a steady state before the arc pulse is applied. The gas pulse is produced by a fast opening magnetic valve, which opens in less than 200 μsec and dumps the contents of a high-pressure plenum chamber into an annular reservoir. The gas then flows continuously into the accelerator through a set of twelve conical nozzles that are fed by the reservoir. Because the length of the arc pulse is short compared to the time scale of variations in the gas flow, the flow is effectively constant during the arc pulse.

The vacuum chamber is a stainless steel tank, roughly cylindrical in shape, with a diameter of 1.2 m and a length of 2.4 m. The accelerator is mounted on the axis of the tank, with its rear surface about 20 cm from the tank wall. A 16-in. oil diffusion pump with a cold trap produces a background pressure of approximately 10^{-6} torr between arc pulses. Since the transit time for the neutral gas atoms to travel downstream to the vacuum chamber wall and back to the accelerator is long compared to the time required for the entire operating sequence, the accelerator is operating in a hard vacuum throughout its pulse.

Probes are mounted on a hydraulically driven carriage that is movable in the radial and axial directions. It is possible to position the probes within 1 mm of a desired position by means of external controls.

B. External Characteristics

Initial observations of the arc current and voltage provided convincing evidence that the pulsed arc attained steady-state operation within 200 μsec after the main pulse line was fired. Figure 3 shows the time dependence of the arc current on the upper trace and arc voltage on the lower trace. The composite photograph shows overlaid oscilloscope traces for three

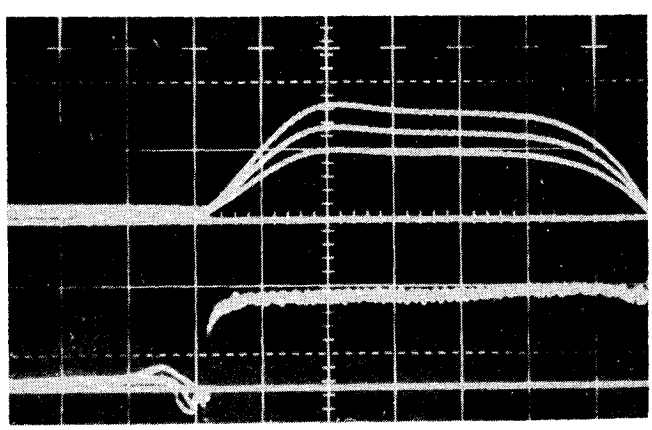

Fig. 3 Photograph of overlaid oscilloscope presentations for three successive machine pulses showing the time dependence of the arc current on the upper trace (1000 amp/div) and arc voltage on the lower trace (50 v/div). (Time sweep from right to left).

successive machine pulses, each with a different value of pulse line charging voltage. The magnetic bias field is held fixed for all three pulses. The arc voltage is clearly insensitive to the variations in arc current. The arc voltage does increase, however, with increasing magnetic bias field as shown in Fig. 4. These characteristics are very similar to those observed in conventional steady-state MPD arcs.

In summary, the pulsed arc does attain a steady-state mode of operation which, at least externally, strongly resembles the operating mode of the conventional MPD arcs.

C. Standard Operating Conditions

The objective of this experiment, a detailed investigation of the internal arc region, requires the correlation of data obtained from several different diagnostic surveys. Since meaningful correlations are possible only if the observations are made under identical conditions, the following operating parameters were adopted as "standard conditions": Gas—Argon, $m = 0.02$ g/sec, $I = 550$ amp, $V = 75$ v, $B_{z0} = 2200$ gauss; where m = mass flow rate, I is the arc current, V is the arc voltage and B_{z0} denotes the value of the maximum axial magnetic field in the plane of the bias field coil. The shape of the magnetic field is shown in Fig. 5. The coordinate system that will be used in the following discussion is also shown.

III. Internal Arc Characteristics

A. Current Distribution

Observations made with magnetic probes show that the current distribution in the internal arc region is not azimuthally uniform. A complete mapping of the local current density has been obtained using small Rogowski coil probes.[6] The output from a Rogowski coil probe positioned at a radius of 3.5 cm (about 8 mm from the anode wall) is shown in Fig. 6 for several different axial positions. Most of the current is localized near the end of the anode ($Z = 10.5$ cm) and the distribution has the shape of a radial spoke which rotates in the $J_r \times B_z$ direction.[7] Under standard conditions the rotation frequency is about 40 kc and seems to be proportional to the product IB as shown in Fig. 7. Similar behavior has been observed in conventional steady-state MPD arcs.[8,9]

High pressure rotating arcs in similar geometries have been observed to have a spiral shape in the R-θ plane.[10,11] Correlated observations with two probes were made in an attempt to detect comparable behavior in the MPD arc; however, no spiralling of the spoke was found in the main body of the arc. A detailed survey of the arc with Rogowski coil probes failed to detect an azimuthal current flow in the plasma region. This is an extremely significant observation since several proposed models of the MPD arc rely on an interaction between J_θ and B_R to produce axial acceleration of the plasma.[12]

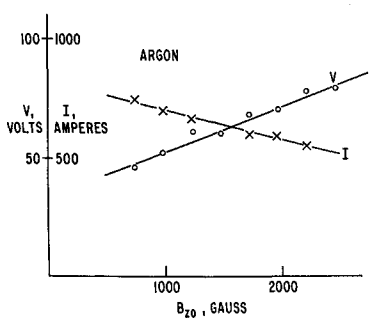

Fig. 4 Arc voltage and arc current as functions of the magnetic bias field. B_{z0} is the magnitude of the field in the plane of the magnetic field coil.

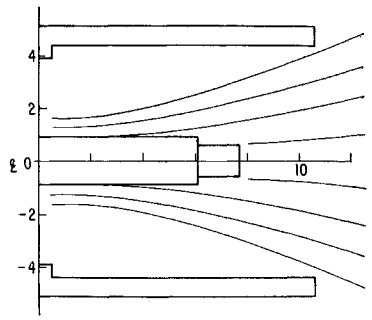

Fig. 5 Magnetic flux lines.

B. Electron Temperature

A collimated telephoto lens was mounted on a spectrometer making it possible to spatially analyze the radiation from the arc. In a spectroscopic survey from 4000 Å to 5010 Å only AII lines were observed. The line intensities emitted from the spoke were an order of magnitude greater than emissions from any other region of the arc or exhaust plume.

The electron temperature of the plasma in the current spoke has been determined by measuring the relative line intensities of sixteen AII spectral lines. Thirteen of the lines were selected because their transition probabilities have been measured experimentally.[13] The remaining three lines were chosen because they have relatively high-excitation energies which increase the sensitivity of the electron temperature measurement. The oscillator strengths calculated by Griem[14] in the L–S approximations were used to determine the transition probabilities for these lines. Since deviations from L–S coupling are expected to decrease as the excitation energy increases, the approximation should be fairly good.

The energy levels involved in the transitions are included in a cluster of levels having interlevel gaps of less than an electron volt, therefore the population densities of these levels should be in local thermal equilibrium with each other.[15]

The magnitude of the observed line intensity is then given by

$$I = (CgA/\lambda) \exp(-E/kT) \qquad (1)$$

where g is the statistical weight of the upper state involved in

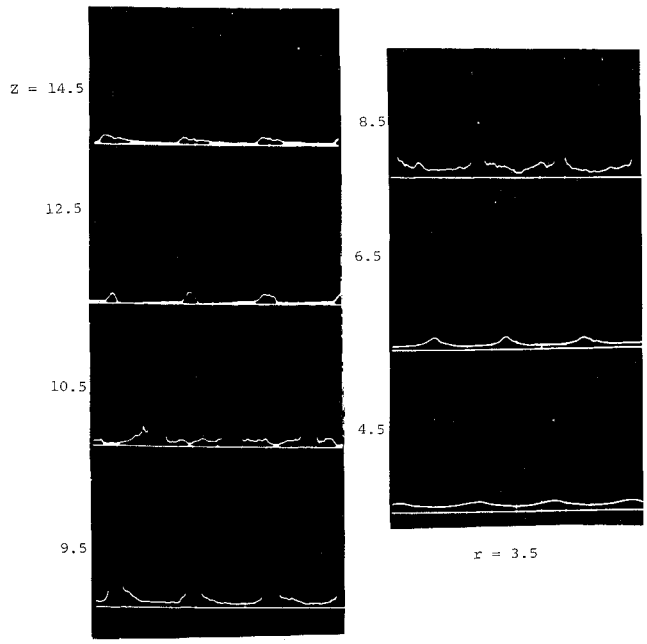

Fig. 6 Oscilloscope traces showing the time dependence of J_r as measured by a Rogowski coil probe for several axial positions and a radius of 3.5 cm. Sweep speed is 10 μsec/-div. Phase is arbitrary.

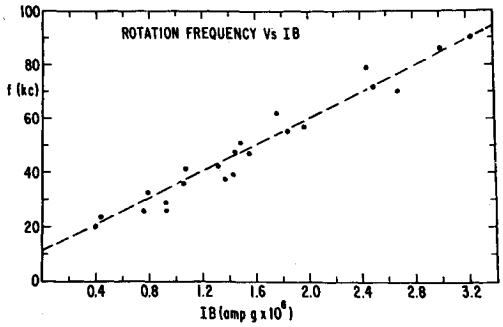

Fig. 7 Spoke rotation frequency vs *IB*.

the transition, A is the transition probability, λ is the wavelength, E is the excitation energy of the upper state, k is the Boltzmann constant, T is the electron temperature, and C is a constant which includes a geometric collection factor.

Taking the log and rearranging, Eq. (1) becomes

$$\ln(\lambda I/gA) = \ln(C) - E/kT \tag{2}$$

Figure 8 is a plot of the experimental values for the left-hand side (LHS) of Eq. (2) as a function of the excitation energies of the observed lines. The data seems to fit a straight line and the slope of the best fit corresponds to an electron temperature of 1.1 ± 0.2 ev.

C. Floating Potential Distribution

The spatial dependence of the floating potential was determined by using a single floating probe. A two-dimensional map of equal floating potential contours in the R–Z plane is shown in Fig. 9. The current spoke lies in the upper half plane of the figure. All potentials are measured with respect to the cathode.

The difference between the floating potential and the actual plasma space potential is given by

$$V_f - V_s = -(kT_e/e)\ln(C_e/4u_i) \tag{3}$$

where V_f is the floating potential, V_s is the space potential, kT_e/e is the electron temperature in ev, c_e is the mean electron thermal speed and u_i is the average ion velocity relative to the probe. The value of the right-hand side (RHS) of Eq. (3) is between 3 and 4 v, therefore, the potentials given in Fig. 9 are within 4 v of the actual space potentials.

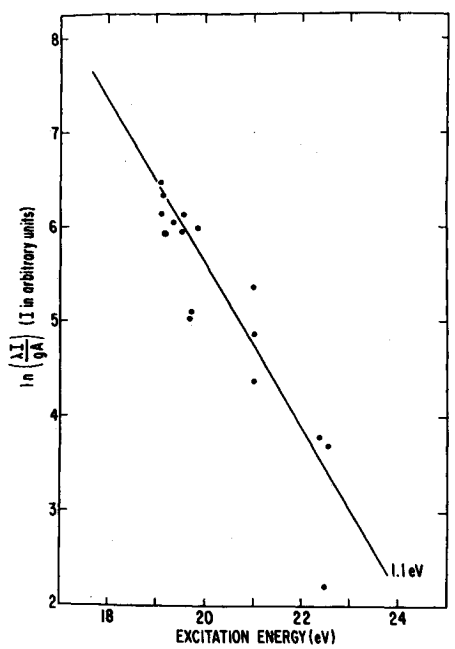

Fig. 8 Plot of ln ($\lambda I/gA$) vs excitation energy for spectral lines of Argon II.

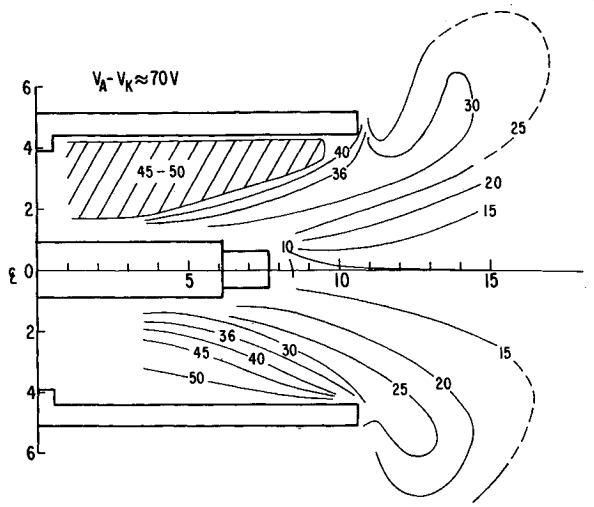

Fig. 9 Contours of equal floating potential. The current spoke is located in the upper half plane.

Since the total voltage drop across the arc is about 70 v, it is clear that near the end of the anode, where the maximum current density is located, there exists a thin anode sheath in which a potential drop of 30 v occurs. Though the sheath thickness is less than 2 mm, approximately half of the input power is dissipated there or at the anode surface.

D. Anode Sheath Current

The presence of the large radial electric field in the anode sheath and the axial magnetic bias field should cause the electrons to drift in the azimuthal direction with a velocity

$$v_\theta = E_R/B_z \tag{4}$$

The ions in the sheath will not experience a similar drift because their gyro radius is large compared to the sheath thickness. The net result is an azimuthal current flow in the sheath.

Because of the small sheath thickness (<2 mm) it is difficult to measure the potential and current distributions in that region. The net anode sheath current, however, can be detected and measured via the magnetic field that it produces outside of the sheath. Measurements of the local axial magnetic field indicate that there is a net azimuthal current flow of about 50 amp within the anode sheath.

IV. Structure of the Plasma Spoke

A. General

With the arc observed to have the form of a rotating spoke, the remaining work was directed toward a detailed analysis of the internal spoke structure. Because of the lack of symmetry, a complete description would be a very formidable task requiring three-dimensional mappings of all measurable plasma properties. Instead, therefore, attention was focused on a limited spatial region centered about a point at a radius of $R = 3.0$ cm and an axial position of $Z = 10.0$ cm. This region is located near the downstream end of the anode where the maximum current density occurs and at a radius large enough so that good spatial resolution is possible.

In the discussion that follows it sometimes is necessary to distinguish between the plasma spoke and the current spoke. The plasma spoke is somewhat broader in azimuth and is displaced slightly ahead of the current spoke in the direction of azimuth motion.

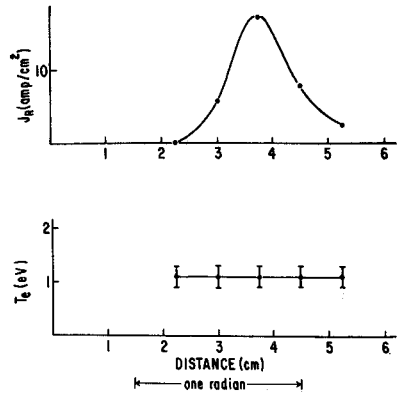

Fig. 10 Radial arc current density and electron temperature vs azimuthal distance at a radius of 3.0 cm.

B. Electron Temperature Distribution

The electron temperature measurement described earlier has been repeated at several points within the spoke with the same result,

$$T_e = 1.1 \pm 0.2 \text{ ev}$$

The observed electron isothermal region extends from a radius of $R = 2.0$ cm to $R = 4.0$ cm. Its azimuthal extent at a radius of $R = 3.0$ cm is shown in Fig. 10. The radial component of the arc current density is included as a reference. In this presentation the current spoke is moving from right to left with a velocity of 7.5×10^5 cm/sec.

Electron temperature measurements were not possible outside of the plasma spoke because the spectral line intensities were too low.

C. Azimuthal Plasma Velocity

Negatively biased Langmiur probes have shown that there is a region of substantial plasma density moving azimuthally just ahead of the current spoke. In this region the radial and axial components of the generalized Ohm's law[16] reduce to

$$E_R = V_\theta B_z \tag{5}$$

and

$$E_z = V_\theta B_R \tag{6}$$

Simplification occurs because there is no current flow in this region and the components of the electron pressure gradient in the radial and axial directions are negligible.

Using Eqs. (5) and (6) it is possible to calculate the azimuthal plasma velocity in two ways from easily measurable field quantities. In both cases the azimuthal plasma velocity is equal to the observed velocity of the current spoke within experimental error which is about 20%.

D. Plasma Density and Velocity Profiles

The components of the plasma flux $n\mathbf{v}$ were measured using a double plane Langmuir probe with two plane electrodes located on opposite sides of the probe. The electrode potentials were maintained strongly negative with respect to the plasma space potential so that all electrons were repelled and all ions moving toward the electrodes were collected.

If the plasma is streaming relative to the probe, the currents collected by the two electrodes will not in general be equal. Consider the case shown in Fig. 11 in which the plasma is directed normally toward the front electrode. The ion velocity distribution is shifted to the right as shown and the current density collected by the front electrode is j_F given by

$$j_F = e\int_0^\infty v_x f(v_x)dv_x \tag{7}$$

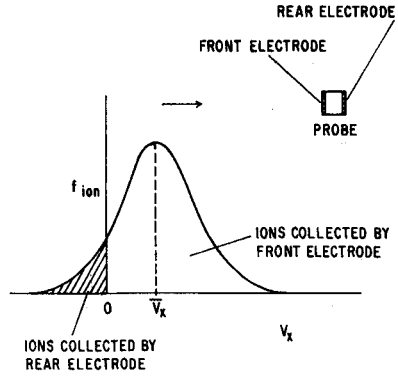

Fig. 11 Portions of the one-dimensional ion velocity distribution collected by the front and rear electrodes of the double plane Langmuir probe.

where $f(v_x)$ is the one-dimensional ion velocity distribution. Equation (7) can be rewritten as

$$j_F = e\int_{-\infty}^{\infty} v_x f(v_x) - e\int_{-\infty}^{0} v_x f(v_x)dv_x$$

or

$$j_F = ne\bar{v}_x + j_R \tag{8}$$

where $\bar{v}_x$ is the mean plasma streaming velocity component normal to the electrode surfaces and j_R is the ion current density collected by the rear electrode. The negative sign occurs in the definition of j_R because the rear electrode is collecting ions moving in the negative direction. The component of plasma flux normal to the electrode surfaces is then obtained from Eq. (8),

$$n\bar{v}_x = (j_F - j_R)/e \tag{9}$$

Figure 12 shows the radial dependence of the ion saturation current densities to the front and rear electrodes of a probe positioned at the end of the anode, Z = 10.5 cm, and oriented azimuthally. Since the azimuthal plasma flux is

$$n\bar{v}_\theta = (j_F - j_R)_\theta/e \tag{10}$$

it is clear from the data of Fig. 12 that the azimuthal plasma flux is approximately proportional to the radius. This implies that the ion density is nearly independent of radius, since

$$n\bar{v}_\theta = n\omega R \tag{11}$$

where ω is the angular frequency of the spoke rotation. An expression for the density n can be obtained by combining Eqs. (10) and (11) and differentiating with respect to R,

$$n = (d/dR)(j_F - j_R)_\theta/e\omega \tag{12}$$

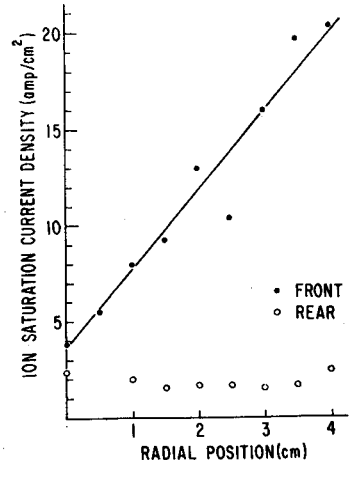

Fig. 12 Radial dependence of the ion saturation current densities to the front and rear electrodes of a double plane Langmuir probe positioned at the mouth of the anode, Z = 10.5 cm, and oriented azimuthally.

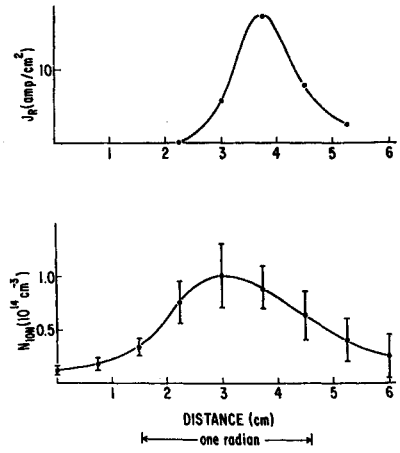

Fig. 13 Radial arc current density and ion density vs. azimuthal distance at a radius of 3.0 cm. Spoke is moving from right to left in this presentation.

Using the slope of the data in Fig. 12 to evaluate the derivation in Eq. (12), the magnitude of the peak plasma density is

$$n = 10^{14}\ \text{cm}^{-3}$$

There is independent evidence for the lack of a radial dependence in the density. The intensities of the AII spectral lines did not vary with radius. Since the electron temperature was found to be independent of radius, the ion density must also be constant.

With the azimuthal plasma velocity assumed equal to that of the current spoke, the density profile in the azimuthal direction was obtained directly from the azimuthal plasma flux observations, since

$$n = (j_F - j_R)_\theta / e\omega R \tag{13}$$

A plot of the ion density vs azimuthal distance is shown in Fig. 13 for a radius of 3.0 cm and an axial position of $Z =$ 10 cm. Again the radial component of the arc current density is included as a reference.

With the ion density profile determined, the double plane Langmuir probe was then oriented in the radial and axial directions in order to measure the profiles of those velocity components. They are given by

$$\bar{v}_R = (j_F - j_R)_R / ne \tag{14}$$

and

$$\bar{v}_z = (j_F - j_R)_z / ne \tag{15}$$

The results are shown in Fig. 14 for a radius of 3.0 cm.

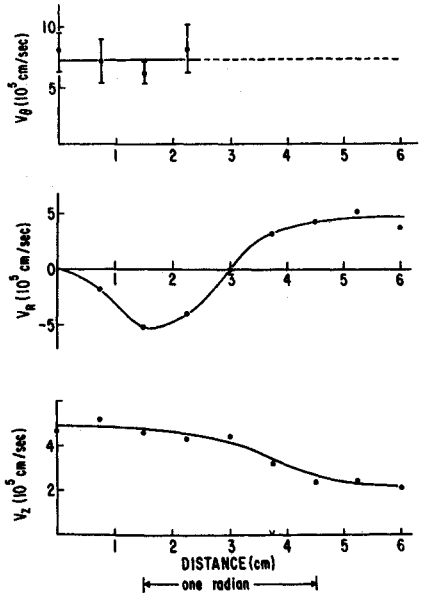

Fig. 14 Plasma velocity components vs azimuthal distance at a radius of 3.0 cm.

Table 1 Comparison of ion energies, measured at several radii, with the stagnation energies of the incoming neutral atoms relative to the moving current spoke

R, cm	kT_i, ev	$E_0 = \frac{1}{2}mv^2R^2$, ev
3.25	12	14
3.0	11	12
2.75	9	10

The radial velocity profile shows the existence of counterstreaming plasma flows. The plasma in front of the current spoke is moving outward, indicating that the centrifugal force is not completely balanced by a radial confining force in this region. In the current spoke, however, the plasma is moving inward, because the confining force exceeds the centrifugal force. The source of the radial confining force will be discussed later. Since the ions in the current spoke are moving inward, they carry a portion of the radial arc current density given by

$$J_{\text{ion}} = ne\bar{v}_R \tag{16}$$

whereas that carried by the electrons is

$$J_{\text{el}} = ne(E_\theta^*/B_z) - ne\bar{v}_R \tag{17}$$

where E_θ^* is the azimuthal component of the electric field in the plasma rest frame. The values of the ion and electron current densities calculated from Eqs. (16) and (17) at $R =$ 3.0 cm on the axis of the current spoke are

$$J_{\text{ion}} = 5\ \text{amp/cm}^2, \quad J_{\text{el}} = 13\ \text{amp/cm}^2$$

thus roughly 30% of the radial arc current is carried by ions and 70% by electrons.

E. Ion Temperature

An order of magnitude estimate of the ion temperature was obtained by rotating the double plane Langmuir probe in the R-plane until the electrode surface was parallel to the net plasma streaming velocity. In this orientation the ion saturation currents to the two electrodes are identical since they are due entirely to the thermal motions. The magnitude of the ion saturation current density is given by Eq. (17)

$$j_{\text{sat}} = 0.5\, ne(kT_e/m_i)^{1/2} \qquad T_i < T_e \tag{18}$$

or

$$j_{\text{sat}} = (1/2\pi)^{1/2} ne(kT_i/m_i)^{1/2} \qquad T_i > T_e \tag{19}$$

depending on whether the ion thermal speed is less than or greater than the Bohm velocity, (kT_e/m_i). Substitution of the measured values of the ion saturation current density j_{sat} and density n gives $kT = 11$ ev. Since the electron temperature has been measured spectroscopically to be 1.1 ev, it is clearly the ion temperature that is of the order of 11 ev.

The same observations were repeated at radii of 3.25 cm and 2.75 cm with the results shown in Table 1. E_0 is the stagnation energy or kinetic energy of the incoming neutral atoms relative to the rest frame of the spoke. The uncertainty in the measured ion temperature is about $\pm 50\%$; therefore, the apparent equality between the ion temperature and the stagnation energy may not be exact, but they are of the same order of magnitude.

The ion-ion mean free path at an energy of 10 ev is approximately 2.5 cm which is nearly 30 times greater than the probe

dimensions. The perturbation produced by the probe can, therefore, be neglected.

The ion saturation current to the rear electrode of the azimuthally oriented probe seems to support the contention that the ion temperature is roughly equal to the stagnation energy. Assuming a Maxwellian velocity distribution for the ions, the ion saturation current density to the rear electrode is

$$j_R = nec_iF(v_s/c_i) \tag{20}$$

where v_s is the plasma streaming velocity and

$$c_i = (2kT_i/m_i)^{1/2}$$

and

$$F(x) = (1/4\pi)^{1/2} \exp(-x^2) - \tfrac{1}{2}x[1 - \operatorname{erf}(x)]$$

The function $F(x)$ is a strongly varying function of x; a factor of two change in $x = v_s/c_i$ produced two orders of magnitude change in $F(x)$. Figure 12 shows the ion saturation current to the rear electrode to be at most a weak function of radius. The ratio (v_s/c_i) must therefore be nearly constant. The value of j_R calculated from Eq. (20), assuming that the ion temperature equals the stagnation energy, is approximately one half of the observed values given in Fig. 12. This agreement is not bad considering the range over which $F(v_s/c_i)$ varies.

V. Summary

The arc has the form of a rotating spoke. The electron temperature is uniform throughout the plasma spoke. The ion density in the spoke is nearly independent of radius and at least an order of magnitude greater than anywhere outside of the spoke.

The azimuthal extent of the plasma spoke is greater than that of the current spoke, with the result that a plasma region exists ahead of the current spoke. This advanced plasma is moving azimuthally with the spoke velocity and appears to be spun out radially by the centrifugal force.

The plasma within the current spoke is counterstreaming radially inward indicating the presence of an inward force greater than the centrifugal force. The ion pressure gradient seems to be the most likely candidate. In accordance with the data listed in Table 1,

$$kT_i = \beta E_0$$

where β is a factor of order one and E_0 is the stagnation energy. Thus

$$kT_i = \tfrac{1}{2}m\omega^2R^2 \tag{21}$$

The radial component of the volume force due to the ion pressure gradient is

$$F_R = -\nabla_R p_i \tag{22}$$

where ∇_R is the radial component of the gradient operator. Since the density n has been observed to be independent of R, Eqs. (21) and (22) together give

$$F_R = -\beta nm\omega^2R = -\beta F_{\text{cent}}$$

where F_{cent} is the centrifugal force per unit volume.

Although no azimuthal currents have been detected in the body or the arc, a current of about 50 amp has been observed to flow azimuthally in the anode sheath. The resulting $J_\theta B_z$ force is directed inward and is of sufficient magnitude to balance the net centrifugal force or equivalently to support the ion pressure gradient. The ions seem to carry about 30% of the radial arc current and the electrons carry the remaining 70%.

References

[1] Ducati, A. C., Giannini, G. M., and Muhlberger, E., "Experimental Results in High-Specific-Impulse Thermo-Ionic Acceleration," *AIAA Journal*, Vol. 2, No. 8, Aug. 1964, pp. 1452–1454.

[2] Patrick, R. M. and Schneiderman, A. M., "Performance Characteristics of a Magnetic Annular Arc," *AIAA Journal* Vol. 4, No. 2, Feb. 1966, pp. 283–290.

[3] Cann, G. L., "Annular Magnetic Hall Current Accelerator," AIAA Paper 64-670, Philadelphia, 1964.

[4] Grossman, W., Hess, R. V., and Hassan, H. A., "Experiments with a Coaxial Hall Current Plasma Accelerator," *AIAA Journal*, Vol. 3, No. 6, June 1965, pp. 1034–1039.

[5] Bennett, S. et al., "MPD Arc Jet Engine Performance," AIAA Paper 65-296, San Francisco, 1965.

[6] Wright, E. S., "The Design and Development of Rogowski Coil Probes for Measurement of the Current Density Distribution in a Plasma Pinch," Rept. 740, June 1965, Dept. of Aerospace and Mechanical Sciences, Princeton Univ., Princeton, N. J.

[7] Ekdahl, C., Kribel, R., and Lovberg, R., "Internal Measurements of Plasma Rotation in an MPD Arc," AIAA Paper 67-655, Colorado Springs, 1967.

[8] Larson, A. V., "Experiments on Current Rotations in an MPD Engine," *AIAA Journal*, Vol. 6, No. 6, June 1968, pp. 1001–1006.

[9] Connolly, D. G. et al., "Low Environmental Pressure MPD Arc Tests," *AIAA Journal*, Vol. 6, No. 7, July 1968, pp. 1271–1276.

[10] Adams, V. W., "The Influence of Gas Streams and Magnetic Fields on Electrical Discharges. Part I: Arcs at Atmospheric Pressure in Annular Gaps," R.A.E. TN Aero. 2896, June 1963, Great Britain Aeronautical Research Council.

[11] Jedlicka, J. R., "The Shape of a Magnetically Rotated Electric Arc in an Annular Gap," TN D-2155, Oct. 1964, NASA.

[12] Cann, G. L. and Marlotte, G. L., "Hall Current Plasma Accelerator," *AIAA Journal*, Vol. 2, No. 7, July 1964, pp. 1234–1241.

[13] Olsen, H. N., "The Measurement of Argon Transition Probabilities Using the Thermal Arc Plasma as a Radiation Source," *Journal of Quantitative Spectroscopy and Radiative Transfer*, Vol. 3, No. 1, Jan. 1963, pp. 59–76.

[14] Griem, H. R., *Plasma Spectroscopy*, McGraw-Hill, New York, 1964, pp. 363–421.

[15] Griem, H. R., "Validity of Local Thermal Equilibrium in Plasma Spectroscopy," *Physical Review*, Vol. 131, No. 3, Aug. 1, 1963, pp. 1170–1176.

[16] Spitzer, L., *Physics of Fully Ionized Gases*, 2nd ed., Interscience, New York, 1962, p. 28.

[17] Bohm, D., "Minimum Ionic Kinetic Energy for a Stable Sheath," *The Characteristics of Electrical Discharges in Magnetic Fields*, edited by A. Guthrie and R. K. Wakerling, McGraw-Hill, New York, 1949, pp. 77–86.